Applied Catalysis B: Environmental 226 (2018) 544–553

Contents lists available at ScienceDirect

Applied Catalysis B: Environmental

journal homepage: www.elsevier.com/locate/apcatb

Selective photocatalytic CO_2 reduction to CH_4 over Pt/In_2O_3: Significant role of hydrogen adatom

Yabo Wang[a], Jie Zhao[b,*], Yingxuan Li[b], Chuanyi Wang[a,c,**]

[a] School of Chemistry and Chemical Engineering, Shihezi University, Shihezi, Xinjiang 832003, China
[b] School of Environmental Sciences and Engineering, Shaanxi University of Science & Technology, Xian, Shaanxi 710021, China
[c] Laboratory of Environmental Sciences and Technology, Xinjiang Technical Institute of Physics and Chemistry, Key Laboratory of Functional Materials and Devices for Special Environments, Chinese Academy of Sciences, Urumqi, Xinjiang 830011, China

ARTICLE INFO

Keywords:
Photocatalytic CO_2 reduction
Metallic Pt
the selectivity to CH_4 production
Atomic hydrogen reservoir

ABSTRACT

The selectivity of photocatalytic CO_2 reduction to CH_4 can be enhanced over Pt-decorated semiconductors, which is commonly attributed to the fact that a Schottky junction is formed, thus enhancing photoinduced electron lifetime. However, it is difficult to understand why the yield of CO—the other product of photocatalytic CO_2 reduction—is decreased only in terms of photoinduced electron lifetime. In this work, the mechanism of Pt-promoted CH_4 formation was probed again in a gas-solid system of photocatalytic CO_2 reduction over highly-dispersed-Pt decorated In_2O_3 nanorods (Pt/In_2O_3). It was found that the presence of Pt modulates the surface property of In_2O_3 due to electronic and steric effect, resulting in a loss of HCO_3^-, b-CO_3^{2-} and m-CO_3^{2-} species for the coadsorption of CO_2 with H_2O. However, this is not directly related with the high CH_4 selectivity and low CO yield on the Pt/In_2O_3 photocatalysts. Photocatalytic reductions of CO, HCOOH, CH_2O, and CH_3OH as well as photocatalytic CO_2 reduction over photocatalysts with different H_2 uptakes confirm that H adatoms derived from H_2 or H_2O dissociation on Pt play a key role in the formation of CH_4. Low H_2 dissociation barrier on Pt and weak H—Pt bond facilitate the bonding of C in CO_2 with H, thus restraining CO production. In other words, the metallic Pt acts as atomic hydrogen reservoir that supplies sufficient and readily available protons for CH_4 formation over Pt-decorated semiconductors. The present work offers a new window to explore non-noble metals or their alloys with stability in air and high dissociation ability to H_2 or H_2O as a replacement of Pt for CO_2 photoreduction to CH_4.

1. Introduction

Photocatalytic CO_2 reduction is gaining wide interest because it is a promising "green chemistry" route driven by sunlight for the direct conversion of CO_2 into value-added fuels [1–5]. Both liquid-(HCOOH, HCHO, and CH_3OH) and gas-phase (CH_4) products have been detected under ambient conditions in liquid-solid system where photocatalysts are dispersed in a CO_2-saturated aqueous solution [6]. CO and CH_4 are commonly produced at the solid–gas interface of photocatalysts and CO_2 [7,8], while H_2 generation derived from water is a competing process accompanying the formation of CO and CH_4 [9]. The solid-gas reaction mode significantly facilitates the separation of photocatalytic materials, products, and reactants. However, it suffers from difficulty in controlling the selectivity to CH_4 production that has a higher heat of combustion [2]. The reduction of CO_2 to CO requires two photoinduced electrons with potential level more negative than −0.48 eV versus normal hydrogen electrode (NHE) at pH = 7 [9], while CH_4 production needs eight photoinduced electrons and eight protons, involving multiple reaction steps with reduction level of −0.24 eV. Although photocatalytic CO_2 reduction to CH_4 is thermodynamically favorable, high selectivity to CH_4 production is hardly achieved over most photocatalysts [10].

Several strategies have been proposed to enhance CH_4 production selectivity, such as surface modifications, ion dopings, developing new type catalysts and metal cocatalysts. For example, hydrophobic modification of TiO_2–SiO_2 surface was used to enhance CO_2 adsorption, thus facilitating the selective generation of CH_4 from CO_2 [4]; Tahir et al. demonstrated that doping In(III) in TiO_2 remarkably increased the yield of CH_4, which was ascribed to effective charge separation and inhibited recombination of photogenerated electron–hole pairs [11]. Some unconventional photocatalysts, such as $LaPO_4$ nanorods [3], Zn_2GeO_4 Nanoribbons [12], SAPO-5 nanosheets [13], β-SiC [14], and so on

* Corresponding author.
** Corresponding author at: School of Chemistry and Chemical Engineering, Shihezi University, Shihezi, Xinjiang 832003, China.
E-mail addresses: zhaojiehj@sust.edu.cn (J. Zhao), cywang@ms.xjb.ac.cn (C. Wang).

https://doi.org/10.1016/j.apcatb.2018.01.005
Received 19 September 2017; Received in revised form 28 December 2017; Accepted 3 January 2018
Available online 04 January 2018
0926-3373/

[15,16], were explored and exhibited a relatively high CH_4 production selectivity. Among the above stated strategies, metal cocatalyst has been a popular technique since Kraeutler and Bard first introduced Pt onto TiO_2 for photocatalytic CO_2 reduction in 1978 [17,18]. Up to now, it was also found that the enhanced CH_4 production selectivity was obtained using other noble metals (such as Pd, Ru, Rh, Ag and Ir) as cocatalysts with a common character of high chemical stability in air [5,19]. For Pt-semconductor photocatalysts, the enhanced CH_4 production selectivity is usually attributed to an increase in photoinduced electron lifetime, owning to the formation of Schottky junctions at the Pt-semconductor interface [20–24]. Note the fact that the CO yield is decreased accompanying the increase in CH_4 production selectivity. In principle, CO yield should be also increased when the number of photoinduced electrons was increased on the surface of Pt-semconductor photocatalysts, since the generation of CO is dynamically more favorable. Moreover, there is no evidence indicating that the decreased CO yield was attributed to the fast transformation of CO to CH_4 [24]. In other words, the experimental observations of the high selectivity to CH_4 production and low CO yield can not be fully explained in terms of the photoinduced electron lifetime at Pt-semconductor interfaces.

In the present work, highly-dispersed-Pt decorated In_2O_3 nanorods with a conduction-band bottom potential energy of -0.62 eV vs. NHE were prepared using a wet chemical method in conjunction with photodeposition, where an acid and alkali neutralization reaction of In $(OH)_3$ with H_2PtCl_6 was involved to enhance Pt dispersion. The mechanism of Pt-promoted CH_4 formation were explored again in a gas-solid system of photocatalytic CO_2 reduction. The addition of Pt leads to a loss of bicarbonates, bidentated carbonate and monodentated carbonate species for the coadsorption of CO_2 with H_2O on the surface of In_2O_3. However, this is not related with the high CH_4 selectivity and reduced CO yield over Pt/In_2O_3. The photocatalytic reductions of the intermediate products of CO_2 reduction such as CO, HCOOH, CH_2O, and CH_3OH as well as photocatalytic CO_2 reduction over photocatalysts with different H_2 uptakes confirm that H adatoms derived from dissociation adsorption of H_2 or H_2O reactant on metallic Pt play a key role in CH_4 formation, which, plus the prolonged photoinduced electron lifetime, would well explain the experimental observations of the enhanced selectivity to CH_4 and low CO yield over Pt/In_2O_3.

2. Experimental

2.1. Synthesis of In_2O_3 and Pt/In_2O_3

$In(OH)_3$ nanorods were prepared by following a previously reported protocol [7,25]. Specifically, 50 g of urea and 6 g of $InCl_3$ were dissolved in 200 mL of deionized water. The aqueous solution was then heated at 80 °C in a water bath under magnetic stirring for 4 h. After being cooled to room temperature, the white product was collected though centrifugation and washed with water to remove unreacted residues. The sample was dried at 80 °C for 4 h to obtain $In(OH)_3$ powder. Following that, 0.5 g of $In(OH)_3$ powders were dispersed into 200 mL of distilled water containing a desired amount of H_2PtCl_6 and 5 mL of methanol. The mixtures were irradiated under UV-light with the wavelength ranging from 200 to 400 nm (a light intensity of 0.120 W cm^{-2}) for 5 h, and the obtained products were collected through centrifugation and washed with water. Finally, the sample materials were annealed at 250 °C for 2 h. As-prepared photocatalysts with Pt loadings 0, 0.5, 1.3 and 2.3 wt% were denoted as In_2O_3, $0.5Pt/In_2O_3$, $1.0Pt/In_2O_3$ and $2.0Pt/In_2O_3$, respectively. For comparison, a $1.0Pt/In_2O_3$-W was prepared using the method of the photodeposition of H_2PtCl_6 on In_2O_3 derived form the calcination of $In(OH)_3$ nanorods at 250 °C, and a $1.0Ag/In_2O_3$ with Ag loading of 1.2 wt% was prepared by using the reduction of $AgNO_3$ with $NaBH_4$ onto In_2O_3.

2.2. Photocatalyst characterization

The chemical compositions of the prepared photocatalysts were analyzed by an ARL-9800 X-ray fluorescence spectrometer (XRF). The surface area and pore size were determined using an Autosorb-IQ-MP autosorption analyzer (Quantachrome), carried out at 77.3 K using N_2 as an adsorbate. The samples were degassed at 473 K for 2 h before measurements. Pore size distribution curves were derived from the branch of adsorption isotherms. X-ray diffraction (XRD) patterns of the samples were collected under ambient atmosphere by a Bruker D8 powder diffractometer with Cu Kα radiation (λ = 1.5408 Å) generated at 40 kV and 30 mA. Transmission electron microscopy (TEM) characterization was performed on a JEOL-JEM 2100 electron microscope.

UV–vis diffuse reflectance spectra (DRS) over a range of 200–800 nm were recorded on a UV–vis spectrophotometer (ShimadzuSolidSpec-3700DUV) with an integration sphere diffuse reflectance attachment. The energy band gaps of the as-prepared samples were calculated using $(\alpha h\nu)^n = \kappa(h\nu - E_g)$, where α is the absorption coefficient, κ is the parameter related to the effective masses associated with the valence and conduction bands, n is 1/2 for the indirect transition, hν is the absorption energy, and E_g is the band gap energy. Plotting $(\alpha h\nu)^{1/2}$ versus hν based on the spectral response gives the extrapolated intercept corresponding to the E_g value. X-ray photoelectron spectroscopy (XPS) study was performed using a VG Microtech MT500 with an Mg-K_X-ray source. All binding energies were referenced to carbon (1s) at 285.6 eV. Time resolved luminescence intensity decays at 395 nm were recorded on a HORIBA Fluorolog-3 molecule fluorometer (France). Those samples were excited by a 300 nm laser light.

IR spectra for the coadsorption of CO_2 and H_2O were recorded with a Nicolet (IS50) spectrophotometer (MCT detector) in the range 4000–1000 cm^{-1} with a resolution of 4 cm^{-1}. The self-supporting wafers (15–20 mg) were annealed in an IR cell at 473 K in Ar for 2 h and evacuated at the same temperature for 1 h. After the IR cell was cooled, CO_2 and H_2O vapor were introduced into the cell.

Adsorptions of H_2 were carried out in a home-made volumetric adsorption system at room temperature. The catalysts were evacuated at 473 K for 2 h before the measurements. After cooling the catalysts to room temperature, doses of H_2 were admitted sequentially and the coverage of H_2 was measured until the equilibrium pressure reached at about 14 kPa. The uptake of H_2 for the saturation coverage on a photocatalyst surface was determined by extrapolating the coverage of isotherm to $P(H_2) = 0$.

2.3. Photoactivity tests

Photocatalytic reductions were carried out in a reactor system connected to a vacuum pump, and a 500 W Hg lamp was used as the light source with a light intensity of 0.120 W cm^{-2}. For each test, 20 mg of a sample catalyst powder was evenly deposited on a circular quartz plate with a diameter of 50 cm and then placed inside the photo-reactor perpendicular to the light beam. 10 mL of gaseous- or 10 μL of liquid-reactant was injected into the vacuum reactor system, and the photocatalytic activities were determined at 298 K for 6 h in each run. The reaction products were monitored at a 60 min interval by an online gas chromatograph (Agilent Technology 7890A GC) equipped with a thermal conductivity detector (TCD) for product analysis of O_2, CO and CH_4 and flame ionization detector (FID) for analyzing products of methanol, formaldehyde, C_2–C_5 hydrocarbons, and so on.

3. Results and discussion

Fig. 1A shows N_2 adsorption-desorption isotherms of the In_2O_3, $0.5Pt/In_2O_3$, $1.0Pt/In_2O_3$, and $2.0Pt/In_2O_3$ photocatalysts. All of the photocatalysts exhibit type-IV adsorption with a hysteresis loop of type H1, indicating the existence of mesopore structures [26]. The isotherms

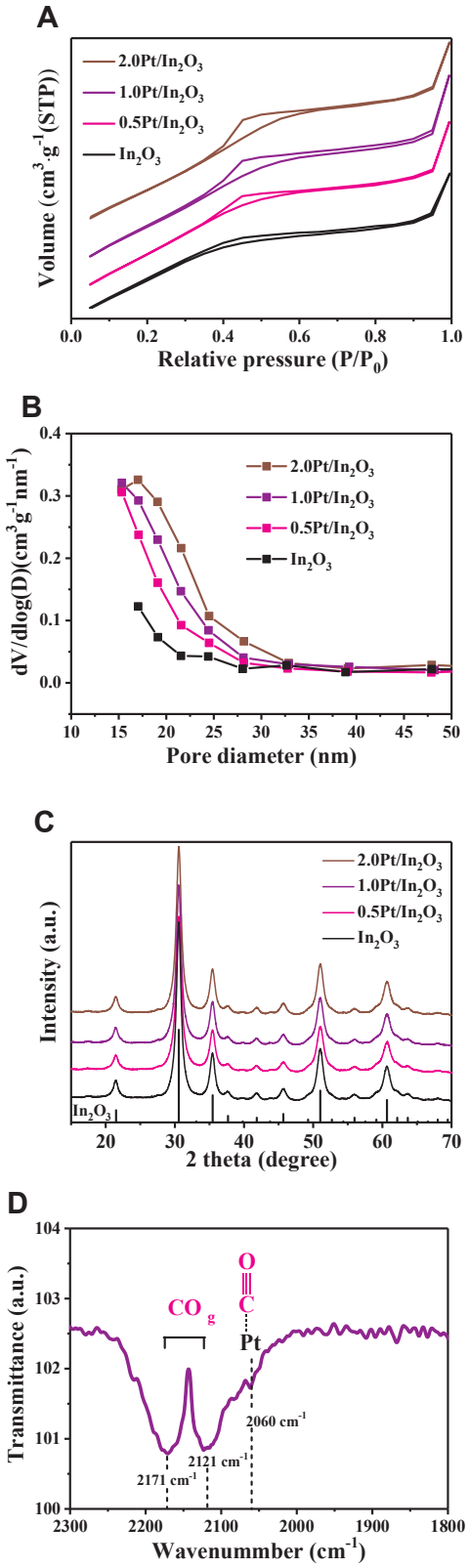

Fig. 1. (A) N_2 adsorption-desorption isotherms, (B) pore size distribution curves and (C) PXRD patterns of the In_2O_3, 0.5Pt/In_2O_3, 1.0Pt/In_2O_3 and 2.0Pt/In_2O_3 photocatalysts. (D) FTIR spectrum for the adsorption of CO at 300 K on the 1.0Pt/In_2O_3. The pore size distribution curve was derived from the adsorption branch of the isotherms.

obviously rise up at a relatively high pressure range of 0.96–1, implying some macropores exist in the photocatalysts [27]. Table 1 summaries BET surface area, pore volume and pore size of the photocatalysts. The

Table 1
Composition, specific surface area, pore volume and average pore size of as-prepared photocatalysts.

Photocatalyst	Catalyst compositions (wt%)		Surface area ($m^2\,g^{-1}$)	Average pore size (nm)	Pore volume ($cm^3\,g^{-1}$)
	In_2O_3	Pt			
In_2O_3	100	0	153.8	17.7	0.14
0.5Pt/In_2O_3	99.5	0.5	162.1	19.4	0.16
1.0Pt/In_2O_3	98.7	1.3	153.5	21.7	0.17
2.0Pt/In_2O_3	97.7	2.3	143.0	22.3	0.16

surface area irregularly changes as Pt loadings increase, which was measured to be 153.8, 162.1, 153.5 and 143.0 $m^2\,g^{-1}$ for In_2O_3, 0.5Pt/In_2O_3, 1.0Pt/In_2O_3 and 2.0Pt/In_2O_3, respectively. Unlike the surface area, the average pore size is slightly increased as the Pt loadings increase, and corresponding pore size distribution curves shift to the large pore size side (Fig. 1B). Powder X-ray diffraction (PXRD) patterns for the photocatalysts indicate a single crystalline phase (Fig. 1C), assigned to the face-centered cubic In_2O_3 (space group #167, *Ia*-3) [25]. Their intensities are not influenced by the addition of Pt. Scherrer analysis of peak broadening shows crystallite sizes of 8–9 nm for In_2O_3 in the photocatalysts. The characteristic peaks of crystalline Pt were not observed for the 0.5Pt/In_2O_3, 1.0Pt/In_2O_3 and 2.0Pt/In_2O_3 photocatalysts, implying Pt particles might be highly dispersed onto In_2O_3.

Fig. 2A and B show scanning electron microscopy (SEM) images of the representative photocatalysts In_2O_3 and 1.0Pt/In_2O_3. A nanorod morphology was observed with lengths ranging from a few hundred nanometers to greater than 1 μm (Fig. 2A). The addition of Pt does not change the morphology of In_2O_3 (Fig. 2B). Transmission electron microscopy (TEM) image of the 1.0Pt/In_2O_3 shows that the nanorods are assembled by small nanoparticles rather than a single crystal (Fig. 2C), which is in line with the character of the larger specific surface area. The crystalline fringes with an interplanar spacing of 0.29 nm can been observed, corresponding to the (222) plane of cubic In_2O_3 crystal, and a Pt particle with a size of about 4 nm is observed in Fig. 2D. As shown Fig. 2S(B), Pt particles are well dispersed on In_2O_3, probably due to the synthetic method for Pt/In_2O_3, where H_2PtCl_6 and $In(OH)_3$ were used as precursors and two hydroxyls on the surface of $In(OH)_3$ would bind a H_2PtCl_6 through a neutralization reaction. Overall, the intrinsic structure of In_2O_3 is barely affected by the addition of Pt.

To illustrate the surface nature of metallic Pt, CO was used as a probe molecule for IR spectroscopy. As shown in Fig. 1D, a CO adsorption band at 2060 cm^{-1} was observed, which can be assigned to CO adsorption in linear configuration [28]. The frequency of the linearly bonded CO is lower than those observed for CO adsorbed over on-top sites of metallic Pt single-crystal surface or metallic Pt nanoparticles supported on some conventional oxide carriers [29,30], indicating a stronger electron donor capacity of metallic Pt in the 1.0Pt/In_2O_3 [28,31–33]. It is suggested that metallic Pt atoms bear high electron density because of support acting as an electron donor or high unsaturated degree of Pt particles. In addition, the peaks at 2190 and 2121 cm^{-1} correspond to the stretching vibration of gaseous CO molecules. No clear evidence shows the existence of bridged/threefold bonded CO whose bands locate at the frequency region of 1800–2000 cm^{-1} [31].

Diffuse reflectance spectroscopy measurements show that the In_2O_3 absorbs light with wavelength below 450 nm (Fig. 3A). The optical bandgap energy of In_2O_3 was estimated to be 3.4 eV (Fig. 1S in Supporting information) [7,34]. The visible-light absorption of the Pt/In_2O_3 samples was slightly improved (the inset of Fig. 3A), which is ascribed to the presence of Pt^{2+} species that will be indicated by the following XPS analysis. Static-state fluorescence (PL) spectroscopic measurements show a peak centered at 395 nm with a marked shoulder around 410 nm for the In_2O_3 and Pt/In_2O_3 photocatalysts (Fig. 3B). The

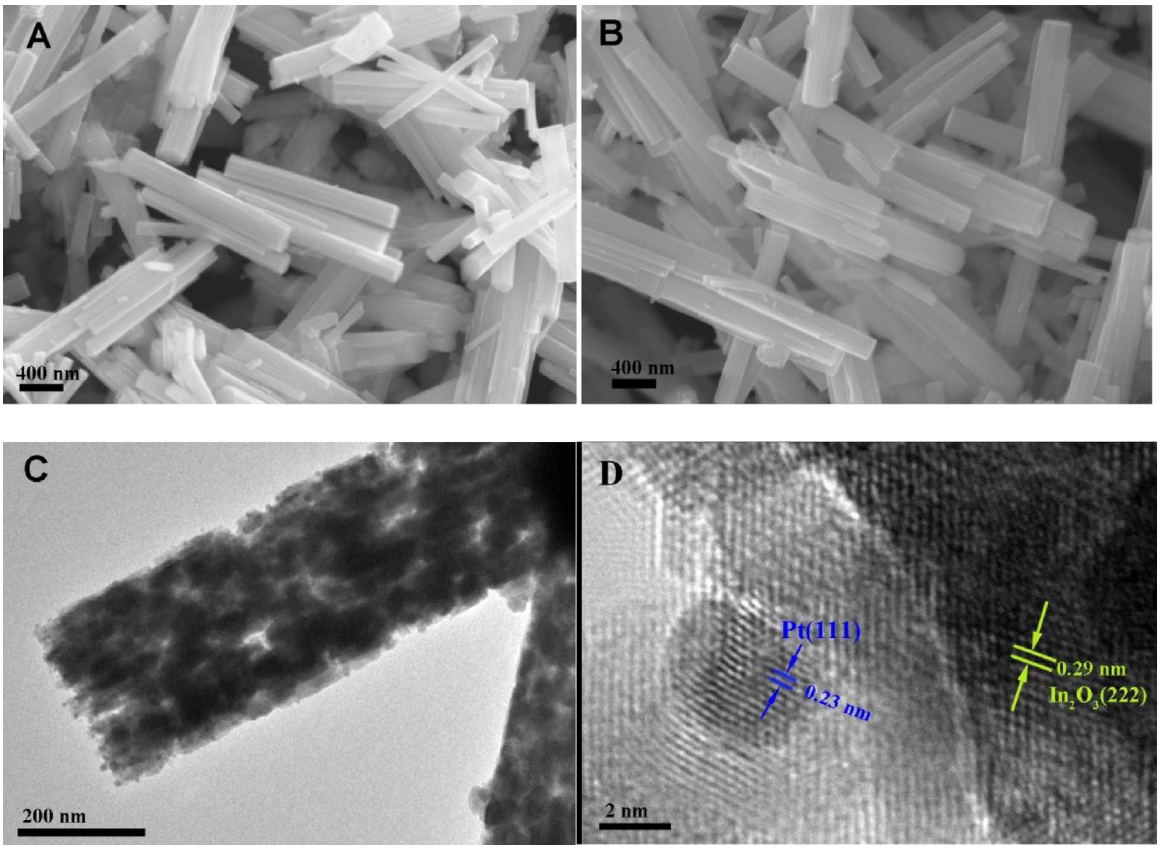

Fig. 2. (A, B) SEM images of the In_2O_3 and 1.0Pt/In_2O_3 photocatalysts, respectively. (C) TEM and (D) HRTEM images of the 1.0Pt/In_2O_3.

peak and its shoulder can be assigned to the near-band-edge emission and shallow-defect-level emission of In_2O_3, respectively [35]. The static-state PL intensity of In_2O_3 declines with increasing Pt loadings. This was attributed to an increase in recombination centers, which was reported to be detrimental for light emission [36]. The PL decay kinetics for the samples at 395 nm after 300 nm excitation were used to examine the recombination rate of the photoinduced electron and hole in photocatalysts. As shown in Fig. 3C, PL decay rate is accelerated with the presence of Pt. In general, the metallic Pt defers the recombination of the photoinduced charge carriers because of the presence of Schottky barriers at Pt-semiconductor interfaces [37], while Pt^{2+} is known as a recombination center of charge carriers [23]. Therefore, the accelerated recombination of photoinduced electron and hole in the Pt/In_2O_3 photocatalysts can be also ascribed to the presence of Pt^{2+}. Note that the lifetime of charge carriers at In_2O_3-metallic Pt interface should be extended.

The performances of photocatalysts were evaluated for CO_2 reduction with H_2O vapor under simulated sunlight irradiation. Besides oxygen, CO and CH_4 were found to be the main products for CO_2 photoreduction, which is in agreement with previous reports [5,7,38,39]. Some possible intermediate products such as HCOOH, CH_2O, and CH_3O were not detected in gas phase, likely due to low abundance of these products, with concentrations below the detection limit of GC instrumentation. As shown in Fig. 4, the yields of CO and CH_4 increase with irradiation time. At 6 h, the CO yield was measured to be about 39.6, 11.5, 8.6 and 15.6 μmol g^{-1}, and the yield of CH_4 was 2.1, 5.6, 21.0 and 18.5 μmol g^{-1} for In_2O_3, 0.5Pt/In_2O_3, 1.0Pt/In_2O_3 and 2.0Pt/In_2O_3, respectively. For comparison, the activities of a commercial TiO_2 and the Pt-decorated TiO_2 with Pt loading of 1% (1.0Pt/TiO_2) were explored and the results are shown in Fig. 4S of the Supporting information. At 6 h, the CO yield was monitored to be 24.2 and 20.6 μmol g^{-1} and the CH_4 yield was 2.7 and 48.8 μmol g^{-1} for TiO_2 and 1.0Pt/TiO_2, respectively. It is evident that CO yield decreases while CH_4 increases after the addition of Pt to either In_2O_3 or TiO_2. At the same time, according to the amount of CO and CH_4, it can be estimated that CO_2 conversion is decreased for 1.0Pt/In_2O_3 and is increased for 1.0Pt/TiO_2. The latter case is in agreement with previous reports [21,23]. Additionally, two control experiments were performed: (1) simulated sunlight irradiation in the absence of catalyst, and (2) irradiation of catalyst and H_2O vapor with simulated sunlight in the absence of CO_2. CO and CH_4 products were not monitored by gas phase analysis in the two experiments, showing the photocatalytic conversion of CO_2.

The enhanced CH_4 yield are commonly attributed to the enhanced photoinduced electron lifetime, due to a Schottky junction formed at the Pt-semiconductor interface [40–42]. Nevertheless, it is difficult to explain the decrease of CO yield only in terms of the prolonged photoinduced-electron lifetime. In dynamics, the reduction of CO_2 to CO requires two electrons, while eight electrons are needed for CH_4 production. As such, the amount of CO should also be increased with the photoinduced electrons lifetime. Moreover, there is no evidence indicating that the decreased CO yield is attributed to the fast conversion of producing CO to CH_4 under light irradiation. Fig. 5S shows the results of photocatalytic reductions of CO_2, and CO with H_2 over the 1.0Pt/In_2O_3, where H_2 instead of H_2O was used as reductant, aiming to suppress the possible oxidation of CO by H_2O-derived oxygen. The CH_4 yield derived from the CO conversion is only 16.4 μmol g^{-1} at 6 h of simulated sunlight irradiation, lower than that of 35.6 μmol g^{-1} for CO_2 photoreduction. Based on the carbon balance, the practical CO yield was estimated to be about 47.7 μmol g^{-1} (16.4 plus 31.3 μmol g^{-1}) at 6 h over the 1.0Pt/In_2O_3, which is still lower than that of 58.4 μmol g^{-1} over the In_2O_3. On the other hand, In_2O_3 is an n-type semiconductor with the conduction band minimum level of −0.62 V versus NHE [43,44]. After being decorated with metallic Pt, an upward band bending would occur at the Pt-In_2O_3 interface due to an apparently higher Fermi level of In_2O_3 than that of Pt [43,45]. Thus, the reduction

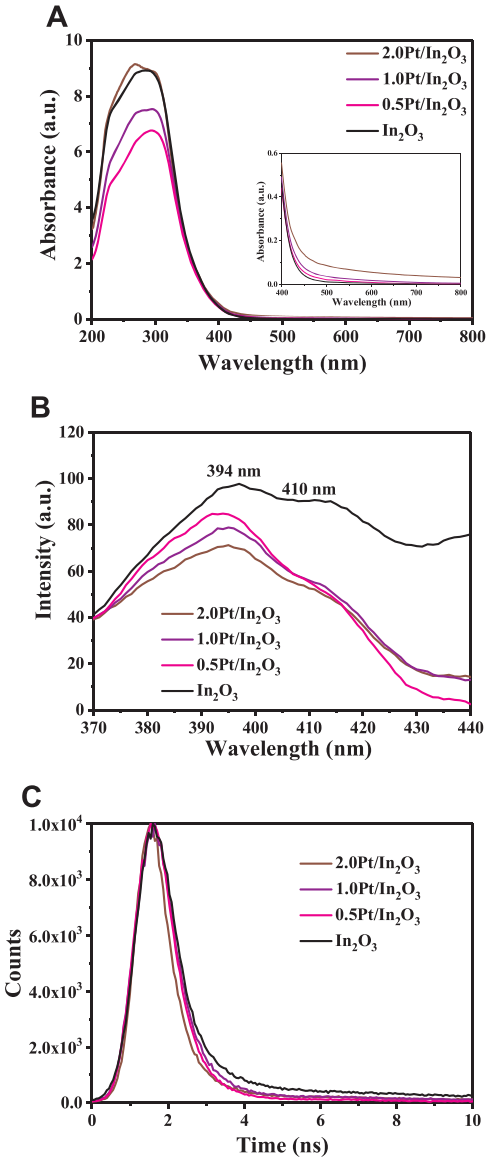

Fig. 3. (A) UV–vis absorption spectra of the In_2O_3, 0.5Pt/In_2O_3, 1.0Pt/In_2O_3 and 2.0Pt/In_2O_3 photocatalysts. (B) Static-state fluorescence spectra of the photocatalysts. (C) The PL decay kinetics for the samples at 395 nm after 300 nm excitation.

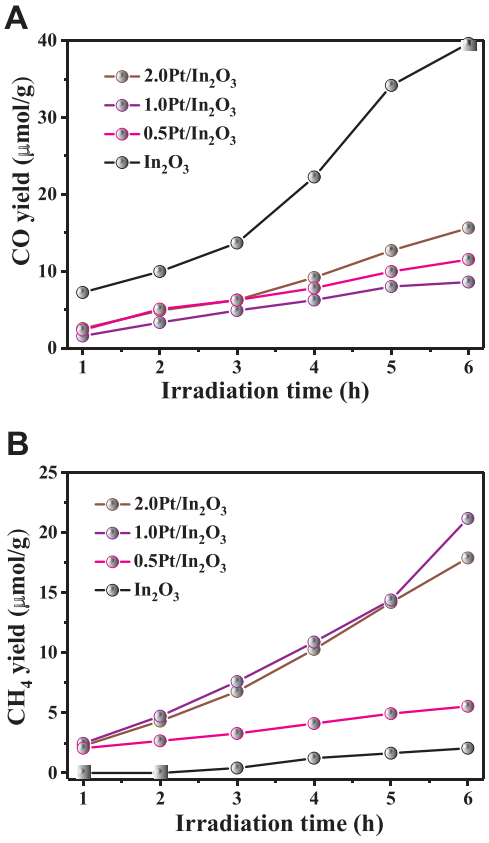

Fig. 4. Yields of CO (A) and CH_4 (B) products for CO_2 photoreduction with H_2O (g) as a function of irradiation time over the In_2O_3, 0.5Pt/In_2O_3, 1.0Pt/In_2O_3 and 2.0Pt/In_2O_3 photocatalysts under simulated light irradiation.

of CO_2 to CO over Pt/In_2O_3, requiring the reduction potential of −0.48 V vs. NHE [46,47], is thermodynamically feasible. At the same time, it is found that low CO yields can be obtained over Pt-decorated semiconductors with different conduction band potentials such as Zn_2GeO_4, CeO_2, $LaPO_4$, C_3N_4, and so on [3,12,48,49], which also implies that the decreased CO yield cannot be ascribed to thermodynamic factor. Therefore, we speculated that there is another reason that jointly support the high selectivity to CH_4 production and low CO yield over Pt-semiconductor catalysts.

Fig. 5 shows XPS spectra of the In_2O_3 and 1.0Pt/In_2O_3 photocatalysts. No impurities other than a very limited amount of contaminants carbon and chlorine were detected (Fig. 5A). The chlorine comes from the raw materials ($InCl_3$ and H_2PtCl_6) in the photocatalyst preparation. Two peaks centered at 444.2 and 451.8 eV can be assigned to the spin–orbit coupling of In $3d_{5/2}$ and $3d_{3/2}$ for In_2O_3 [50]. Corresponding peaks for 1.0Pt/In_2O_3 shift to the high binding energy side by 0.2 eV (Fig. 5B). For O 1s core level XPS, the peak assigned to lattice oxygen of cubic In_2O_3 was observed with a shoulder, shifting from a binding energy of 529.6 for the In_2O_3 to 529.9 eV for the 1.0Pt/In_2O_3 photocatalyst. The shoulder at about 532.4 eV is due to the surface hydroxyl. Pt 4f core level XPS measurement indicates that Pt^{2+} and Pt^0 are present with Pt^0 atomic ratio of 29% relative to total Pt on the surface of 1.0Pt/In_2O_3 (Fig. 5D) [51]. Pt^{2+} comes from the partial reduction product ($PtCl_2$) of H_2PtCl_6. These results indicate that the electron densities of In and O on the surface of 1.0Pt/In_2O_3 is slightly decreased relative to those on In_2O_3, leading to the higher binding energies, which can be explained in terms of a higher electronegativity of Pt (2.28) than that of In (1.78). When Pt species contacts with the surface of In_2O_3, the valance electrons of O are attracted by Pt species. Meanwhile, the bonding electrons in In—O will further depart from In atoms via inductive effect.

To illustrate the effect of Pt species on the co-adsorption of CO_2 with H_2O, the FTIR measurements were carried out. As shown in Fig. 6A, the peaks at 1645, 1549, 1510, 1429, 1394, 1338 and 1219 cm^{-1} are observed for In_2O_3, which can be assigned to bicarbonates (HCO_3^-), bidentated carbonate (b-CO_3^{2-}) and monodentated carbonate (m-CO_3^{2-}) species [52–55]. However, these peaks are not observed for the 1.0 Pt/In_2O_3, and 2.0 Pt/In_2O_3 (Fig. 3S). When the Pt loadings is decreased to 0.5%, these peaks with weak intensity reappear (Fig. 6S). Because bicarbonate- and carbonate-like species are active under light irradiation [26], a loss of them might cause a decrease in CO_2 conversion, which explains the aforementioned observation about CO_2 reduction with H_2O over the Pt/In_2O_3 photocatalysts. On the other hand, the molecularly adsorbed CO_2 were all observed on the In_2O_3 and 1.0 Pt/In_2O_3. It is well known that when CO_2 molecule is bonded to the surface oxygen atom of In_2O_3 through its carbon atom, surface m-CO_3^{2-} species is formed (Fig. 6B). If CO_2 is simultaneously bonded to the oxygen and In sites of In_2O_3 through its carbon and oxygen, surface b-CO_3^{2-} species will be formed, and the surface HCO_3^- species is derived from a reaction of CO_2 with surface hydroxyl. CO_2 molecule is bound with In atom of In_2O_3 through its oxygen atom, yielding molecularly adsorbed CO_2

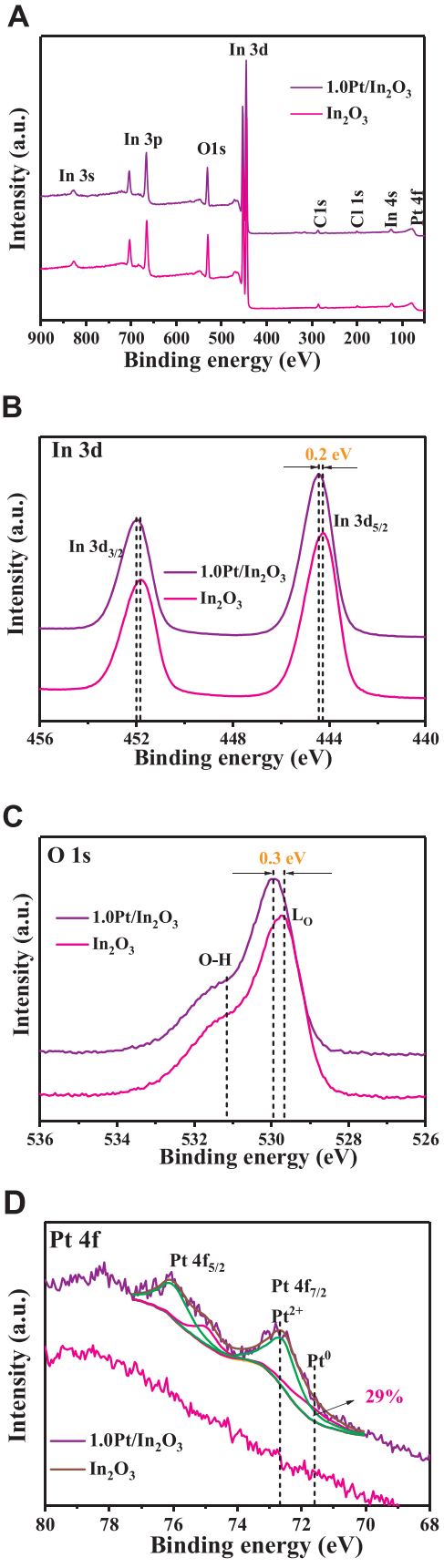

Fig. 5. (A) Survey, (B) In 3d, (C) O 1s, and (D) Pt 4f core level XPS spectra of the 1.0Pt/In_2O_3 and In_2O_3 photocatalysts.

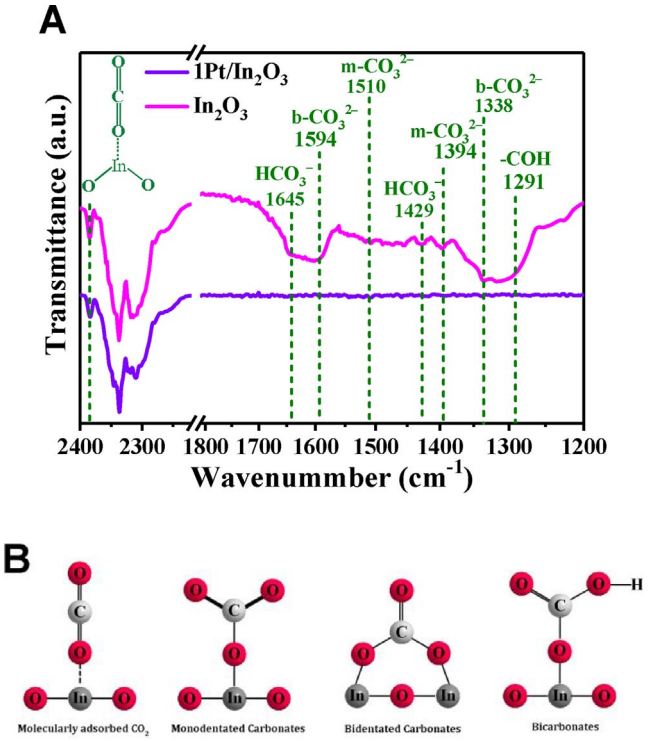

Fig. 6. (A) The FTIR spectra for the coadsorption of CO_2 and H_2O (g) on the 1.0Pt/In_2O_3 and In_2O_3 photocatalysts. (B) Schematic surface species for the coadsorption of CO_2 and H_2O (g) on the photocatalysts.

(Fig. 6B). As such, a loss of HCO_3^-, b-CO_3^{2-} and m-CO_3^{2-} on the Pt/In_2O_3 photocatalysts indicates that the oxygen atoms on the surface of In_2O_3 might be covered by Pt species, which is also implied by the XPS analysis. It should be noted that the HCO_3^-, b-CO_3^{2-} and m-CO_3^{2-} species weren't suppressed for the adsorption of CO_2 on Pt-decorated TiO_2 [21,56,57]. For example, Xiong et al. and Mao et al. reported that the effect of Pt on the CO_2 chemisorption was not obvious over TiO_2 [21,56]. Also, Long et al. reported that CuPd alloy similar to Pt did not prevent the formation of HCO_3^- and carbonate-like species on TiO_2 [57]. More importantly, the high CH_4 production selectivity and low CO yield were also obtained over these reported photocatalysts. Therefore, the lack of HCO_3^-, b-CO_3^{2-} and m-CO_3^{2-} species over Pt decorated In_2O_3 should not be directly related with the high CH_4 selectivity and low CO yield in the work.

To probe whether some intermediate products of CO_2 reduction are influenced by Pt species in photocatalytic CO_2 reduction, leading to the higher CH_4 production selectivity, we evaluated the photocatalytic reduction of intermediate products to CH_4 such as CO, HCOOH, CH_2O, and CH_3O over the In_2O_3 and 1.0Pt/In_2O_3 under simulated sunlight irradiation. In this study, H_2 instead of H_2O was used as reductant, aiming to block the oxidation of these intermediate products by H_2O-derived oxygen. As can be seen from Fig. 7, more CH_4 was produced for photocatalytic CO_2 reduction with H_2 than with H_2O over In_2O_3 and 1.0Pt/In_2O_3. CH_4 was also produced in the reduction of CO, HCOOH, CH_2O, and CH_3O over 1.0Pt/In_2O_3, and its yield was measured to be about 16.4, 7.6, 16.7 and 6.7 μmol g^{-1} under simulated-sunlight irradiation of 6 h, respectively. Unexpectedly, the CH_4 yields derived from intermediate products reduction are obviously lower that of 35.6 μmol g^{-1} for CO_2 reduction, although the reduction of intermediate products requires less photoinduced electrons relative to CO_2 reduction. So far, two pathways for photocatalytic CO_2 reduction were proposed according to whether the hydrogenation or the deoxygenation process is faster [1,47,58]. In the fast-hydrogenation pathway, CO_2 is reduced along the path $CO_2 \rightarrow HCOOH \rightarrow CH_2O \rightarrow CH_3OH \rightarrow CH_4$; while in the fast-deoxygenation pathway, it follows the path $CO_2 \rightarrow$

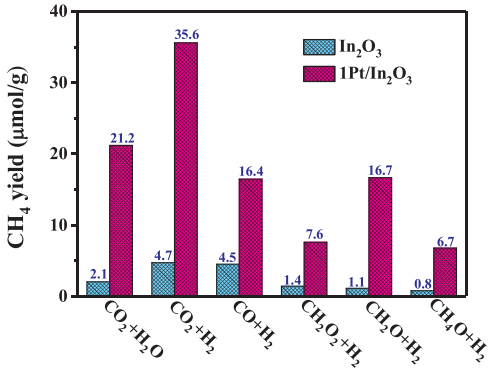

Fig. 7. CH_4 yields for the C1 molecules photoreduction over 1.0Pt/In_2O_3 and In_2O_3 photocatalysts at 6 h of simulated light irradiation.

$CO \rightarrow C\cdot \rightarrow CH_2\cdot \rightarrow CH_3\cdot \rightarrow CH_4$ [59]. Some intermediates in both pathways have been detected [1,58]. For example, carbon radicals signals were detected by ESR spectroscopy [1]. Recent theoretical calculation by Ji et al. shows that photocatalytic CO_2 reduction follows both the fast-hydrogenation and fast deoxygenation pathways [59]. Combining theoretical calculation with the results obtained in the present work, it is plausible that photocatalytic CO_2 reduction indeed proceeds via multiple pathways. In contrast, the reduction of intermediate products might only follow a specific pathway. As a result, more active species for CH_4 formation were produced in CO_2 reduction, leading to the higher CH_4 production yield. On the other hand, the CH_4 yield over the 1.0Pt/In_2O_3 is obviously higher than that over the In_2O_3, regardless of which intermediate product is served as oxidant, implying that the factor of enhancing the CH_4 selectivity might relate with the reductant (H_2 or H_2O). Theoretical calculations indicate that H_2 and H_2O can be dissociatively adsorbed on Pt and In_2O_3 [54,60–63]. For H_2O molecule, H adatom and surface hydroxyl are formed on Pt, and H_2O-derived H and OH are bound to O and In on the surface of In_2O_3, thus forming two hydroxyls. For H_2, homolytic dissociation produces two hydroxyls on In_2O_3 [54,59,63,64], and heterolytic dissociation results in H—In and O—H species on the surface of In_2O_3. Homolytic dissociation is highly energetically favorable. Moreover, the adsorption energies for H_2 and H_2O is higher on In_2O_3 than on Pt, owing to a higher bonding energy of O—H bond than that of Pt—H bond [54,65]. As such, it can be speculated that the transfer of H in Pt—H to CO_2 will overcome a less barrier than that in O—H bond. Therefore, it is suggested that H adatoms play a key role in enhancing CH_4 selectivity over Pt-decorated semiconductors.

To further evidence the significant role of H adatoms to CH_4 selectivity, we evaluated the performance of a set of photocatalysts with different H_2 uptakes for CO_2 reduction to CH_4. Fig. 8A shows coverage vs. pressure of H_2 on the In_2O_3, 1.0Pt/In_2O_3, 1.0Pt/In_2O_3-W and 1.0Ag/In_2O_3 photocatalysts. The ratio of metallic Pt relative to total Pt in the 1.0Pt/In_2O_3-W is about 35%, as indicated by XPS results (Fig. 7S). The uptakes of H_2 increase with pressure on photocatalysts. The saturation coverage of H_2, obtained by extrapolating the coverage of isotherm to P (H_2) = 0, is 2.7, 34.2, 46.1 and 12.6 μmol/g for In_2O_3, 1.0Pt/In_2O_3, 1.0Pt/In_2O_3-W and 1.0Ag/In_2O_3, respectively. Obviously, the H_2 uptake for In_2O_3 is the least. The addition of Pt and Ag promotes the adsorption of H_2. Among the three hybrid photocatalysts, the 1.0Pt/In_2O_3-W shows the highest H_2 uptake. These results indicate that the H_2 dissociative barrier on Pt (or Ag) is significantly lower than that on In_2O_3, which is further evidenced by the following experimental results for the reduction of the In_2O_3 and 1.0 Pt/In_2O_3 photocatalysts (Fig. 8B). The 1.0Pt/In_2O_3 was fully reduced to metallic In in H_2 at 723 K for 2 h. However, the In_2O_3 was not reduced to form In under the same condition. Only a change occurs in color from light gray to dark gray, which is ascribed to In_2O_3 surface reduction. It is well known that H_2 molecule was firstly dissociated to form H atoms before redox reactions. Thus, metallic Pt promoted the dissociation of H_2 molecule to more active H atoms. Fig. 8C and D shows the yields of CO and CH_4 and the selectivity to CH_4 over the photocatalysts for the reduction of CO_2 with H_2. The mean CO yield was measured to be about 58.3, 31.3, 2.7 and 27.4 μmol/g, the mean CH_4 yield was 4.7, 33.6, 51.0 and 12.5 μmol/g for In_2O_3, 1.0Pt/In_2O_3, 1.0Pt/In_2O_3-W and 1.0Ag/In_2O_3, respectively. According to the amount of CO and CH_4, the conversion of CO_2 was calculated to be about 63.0, 64.9, 53.7 and 39.9 μmol/g for In_2O_3, 1.0Pt/In_2O_3, 1.0Pt/In_2O_3-W and 1.0Ag/In_2O_3, respectively. Clearly, the presence of Pt (or Ag) does not promote the conversion of CO_2, only changing the product selectivity. The selectivity to CH_4 was calculated to be 7.4, 51.9, 93.3 and 31.3 for In_2O_3, 1.0Pt/In_2O_3, 1.0Pt/In_2O_3-W and 1.0Ag/In_2O_3, respectively (Fig. 8D). This is positively correlated to the H_2 uptakes by the photocatalysts. Besides, Ag and Pt has a common property of strong dissociation ability to H_2, and high CH_4 selectivities were simultaneously achieved over Ag- and Pt-decorated In_2O_3. The result also indicates the key role of H adatoms in CH_4 formation. It should be noted that the particle size of metallic Pt is another key factor to the selectivity of CO_2 reduction. Wang et al. have investigated the correlation between the Pt particle size and the selectivity of CO_2 reduction over TiO_2 single crystals. It was found that high CO_2 photoreduction efficiency with selective formation of methane was achieved when the Pt particle size is 0.5–2 nm, and the optimal size was found to be around 1 nm. Pt particles on this nanoscale have a suitable Fermi level due to quantum effect, thereby effectively promoting the photoinduced electron transfer [24]. According to the TEM images shown in Fig. 2S, the sizes of Pt particles of the 1.0Pt/In_2O_3 and 1.0Pt/In_2O_3-W samples were estimated to be 3–5 nm, and there is no observable difference in the Pt particle size between 1.0Pt/In_2O_3 and 1.0Pt/In_2O_3-W (Figs. 2S and 3S). Note that on the nanoscale of 3–5 nm quantum effect is not so obvious. Therefore, possible effect of the size of Pt particles on the selectivity to CH_4 was not be considered in the work.

The bonding of CO_2 with H can be seen as thermal chemical process following the photo-activation of CO_2. As such, the selectivity to CH_4 should be influenced by H_2 partial pressure. Therefore, the CH_4 selectivity in different partial pressure ratios of CO_2 to H_2 was evaluated over the 1.0Pt/In_2O_3 sample. As shown in Fig. 8, the CH_4 selectivity decreases with decreasing H_2 partial pressures, further confirming the critical role of H supply in CH_4 formation. In photocatalytic CO_2 reduction, H_2 molecule is oxidated to produce two protons being bound to coordinatively unsaturated oxygens on the surface of In_2O_3. When the protons transfer to the O in CO_2, CO and H_2O will be formed, which is so-called deoxygenation process; If the protons transfer to C in CO_2, the probability of CH_4 formation will be obviously increased, as indicated in Scheme 1. To produce CH_4, the C in CO_2 needs to fight for the protons with the oxygen on the surface of In_2O_3. Notably, the C of CO_2 is at a disadvantage, owing to its electronegativity lower than that of oxygen. However, the presence of metallic Pt cocatalyst will change the unfavorable case. H_2 is first dissociated to form Pt—H bonds on Pt surface. As such, it becomes easy to the capture of protons by the C in CO_2 from Pt—H species, since the electronegativity of C (2.55) is higher than that of Pt. In dynamics, the sufficient and fast proton supply is a prerequisites for CH_4 production, since the formation of CH_4 from CO_2 requires eight protons and multiple steps [66]. The metallic Pt can supply a plenty of H adatoms, and the H adatoms on metallic Pt can be more quickly bound with CO_2 than that on In_2O_3, owing to a relatively weaker bonding of Pt—H. Therefore, the metallic Pt acts as atomic hydrogen reservoir that supplies sufficient and readily available protons for CH_4 production.

In addition, although the CO_2 conversion is not increased over Pt-decorated In_2O_3 photocatalysts in the work, the number of the photoinduced electrons involved in the reduction is actually increased because the number of required electrons for CH_4 production is three times more than that for CO. Thus, the extended lifetime of photoinduced electrons is still an indispensable factor for the enhanced selectivity to CH_4 production, which has been verified in previous studies

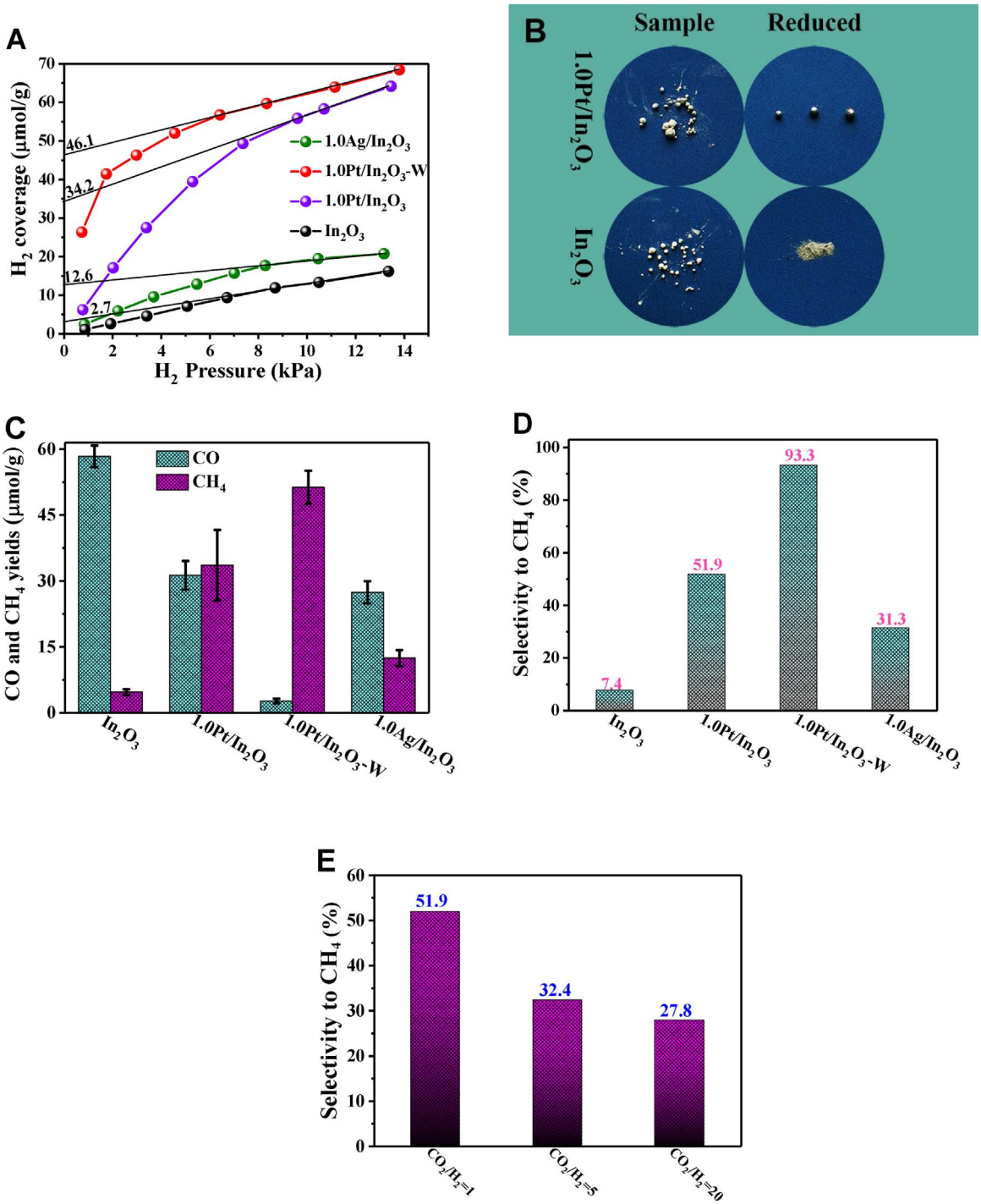

Fig. 8. (A) Coverage vs. pressure of H_2 on the In_2O_3, 1.0Pt/In_2O_3, 1.0Pt/In_2O_3-W and 1.0Ag/In_2O_3. (B) The photograph of the In_2O_3 and 1.0Pt/In_2O_3 photocatalysts before and after reduction in H_2 flow at 723 K for 2 h. (C) Yields of CO and CH_4 products and (D) the selectivity to CH_4 for the photoreduction of CO_2 with H_2 on In_2O_3, 1.0Pt/In_2O_3, 1.0Pt/In_2O_3-W and 1.0Ag/In_2O_3. The error bars represent the standard deviations of three independent measurements of the same sample. (E) The selectivity to CH_4 over 1.0Pt/In_2O_3 in different partial pressure ratios of CO_2 to H_2.

[21,24].

4. Conclusions

In summary, highly-dispersed-Pt decorated In_2O_3 nanorods (Pt/In_2O_3) were prepared using a precipitation method in conjunction with photodeposition, where acidic H_2PtCl_6 and basic $In(OH)_3$ were selected as precursors for enhancing Pt dispersion. The presence of Pt does not change the intrinsic structure of In_2O_3, but modulates the surface property of In_2O_3 due to electronic and steric effect, which results in a loss of HCO_3^-, b-CO_3^{2-} and m-CO_3^{2-} species for the coadsorption of CO_2 with H_2O on Pt/In_2O_3. However, this is not the cause of the high CH_4 production selectivity and low CO yield for photocatalytic CO_2 reduction over Pt/In_2O_3. Photocatalytic CO, HCOOH, CH_2O, and CH_3OH reductions over Pt/In_2O_3 as well as photocatalytic CO_2 reduction over photocatalysts with different H_2 uptakes confirm that H adatoms derived from H_2 or H_2O dissociation on Pt play a key role in the formation of CH_4. Low H_2 dissociation barrier on Pt and weak H-Pt bond facilitate the bonding of C in CO_2 with H, thus restraining CO production. Combining with previous reports [24], it can be concluded

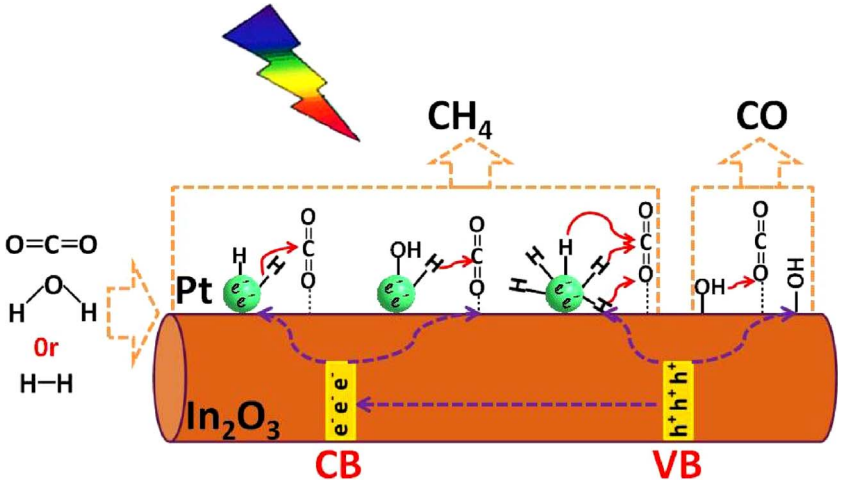

Scheme 1. The probable transfer paths of H adatoms derived form H_2 or H_2O to adsorbed CO_2 over Pt/In_2O_3.

that metallic Pt not only extends photoinduced-electron lifetime but also acts as atomic hydrogen reservoir that supplies sufficient and readily-available protons for CH_4 formation. The two roles by Pt would well explain the experimental results of the high selectivity to CH_4 production and low CO yield over Pt/In_2O_3. The present work deepens the understanding of mechanism for Pt-promoted CH_4 formation over Pt-semiconductor photocatalysts, offering a new window to explore non-noble metals or their alloys with stability in air and high dissociation ability to H_2O or H_2 as a replacement of Pt for CO_2 photoreduction to CH_4.

Acknowledgements

Financial support by the National Nature Science Foundation of China (Grant No. 21473248), the CAS/SAFEA International Partnership Program for Creative Research Teams, and the Youth Talent Support Program of Shaanxi University of Science & Technology is gratefully appreciated.

Appendix A. Supplementary data

Supplementary data associated with this article can be found, in the online version, at https://doi.org/10.1016/j.apcatb.2018.01.005.

References

[1] S.N. Habisreutinger, L. Schmidt-Mende, J.K. Stolarczyk, Angew. Chem. Int. Ed. 52 (2013) 7372–7408.
[2] X. Meng, S. Ouyang, T. Kako, P. Li, Q. Yu, T. Wang, J. Ye, Chem. Commun. 50 (2014) 11517–11519.
[3] B. Pan, S. Luo, W. Su, X. Wang, Appl. Catal. B: Environ. 168–169 (2015) 458–464.
[4] C. Dong, M. Xing, J. Zhang, J. Phys. Chem. Lett. 7 (2016) 2962–2966.
[5] S. Xie, Y. Wang, Q. Zhang, W. Deng, Y. Wang, ACS Catal. 4 (2014) 3644–3653.
[6] D.J. Boston, C. Xu, D.W. Armstrong, F.M. MacDonnell, J. Am. Chem. Soc. 135 (2013) 16252–16255.
[7] L.B. Hoch, T.E. Wood, P.G. O'Brien, K. Liao, L.M. Reyes, C.A. Mims, G.A. Ozin, Adv. Sci. 1 (2014) 1400013.
[8] I.A. Shkrob, T.W. Marin, H. He, P. Zapol, J. Phys. Chem. C 116 (2012) 9450–9460.
[9] T.-D. Pham, B.-K. Lee, J. Catal. 345 (2017) 87–95.
[10] Z. Wang, K. Teramura, Z. Huang, S. Hosokawa, Y. Sakata, T. Tanaka, Catal. Sci. Technol. 6 (2016) 1025–1032.
[11] M. Tahir, N.S. Amin, Appl. Catal. B: Environ. 162 (2015) 98–109.
[12] Q. Liu, Y. Zhou, J. Kou, X. Chen, Z. Tian, J. Gao, S. Yan, Z. Zou, J. Am. Chem. Soc. 132 (2010) 14385–14387.
[13] S.Y. Zhu, S.J. Liang, Y. Wang, X.Y. Zhang, F.Y. Li, H.X. Lin, Z.Z. Zhang, X. Wang, Appl. Catal. B: Environ. 187 (2016) 11–18.
[14] Y. Wang, L. Zhang, X. Zhang, Z. Zhang, Y. Tong, F. Li, J.C.S. Wu, X. Wang, Appl. Catal. B: Environ. 206 (2017) 158–167.
[15] Y. Zhou, Z. Tian, Z. Zhao, Q. Liu, J. Kou, X. Chen, J. Gao, S. Yan, Z. Zou, ACS Appl. Mater. Interfaces 3 (2011) 3594–3601.
[16] E.G. Look, H.D. Gafney, J. Phys. Chem. A 117 (2013) 12268–12279.
[17] B. Kraeutler, A.J. Bard, J. Am. Chem. Soc. 100 (1978) 4317–4318.
[18] M. Anpo, H. Yamashita, Y. Ichihashi, Y. Fujii, M. Honda, J. Phys. Chem. B 101 (1997) 2632–2636.
[19] P. Kar, S. Farsinezhad, N. Mahdi, Y. Zhang, U. Obuekwe, H. Sharma, J. Shen, N. Semagina, K. Shankar, Nano Res. 9 (2016) 3478–3493.
[20] H.L. Li, X.Y. Xu, J. Wang, L.Q. Gao, Int. J. Hydrogen Energy 41 (2016) 8479–8488.
[21] Z. Xiong, Z. Lei, C.-C. Kuang, X. Chen, B. Gong, Y. Zhao, J. Zhang, C. Zheng, Jeffrey C.S. Wu, Appl. Catal. B: Environ. 202 (2017) 695–703.
[22] S. Xie, Y. Wang, Q. Zhang, W. Fan, W. Deng, Y. Wang, Chem. Commun. 49 (2013) 2451–2453.
[23] W.-J. Ong, L.-L. Tan, S.-P. Chai, S.-T. Yong, Dalton Trans. 44 (2015) 1249–1257.
[24] W.-N. Wang, W.-J. An, B. Ramalingam, S. Mukherjee, D.M. Niedzwiedzki, S. Gangopadhyay, P. Biswas, J. Am. Chem. Soc. 134 (2012) 11276–11281.
[25] L. He, T.E. Wood, B. Wu, Y. Dong, L.B. Hoch, L.M. Reyes, D. Wang, C. Kübel, C. Qian, J. Jia, K. Liao, P.G. O'Brien, A. Sandhel, J.Y.Y. Loh, P. Szymanski, N.P. Kherani, T.C. Sum, C.A. Mims, G.A. Ozin, ACS Nano 10 (2016) 5578–5586.
[26] Y. Wang, J. Zhao, T. Wang, Y. Li, X. Li, J. Yin, C. Wang, J. Catal. 337 (2016) 293–302.
[27] J. Zhao, M. Xue, Y. Huang, J. Shen, Catal. Commun. 16 (2011) 30–34.
[28] L. Liu, U. Diaz, R. Arenal, G. Agostini, P. Concepcion, A. Corma, Nat. Mater. 16 (2017) 132–138.
[29] E. Carrasco, A. Aumer, M.A. Brown, R. Dowler, I. Palacio, S. Song, M. Sterrer, Surf. Sci. 604 (2010) 1320–1325.
[30] C. Klvker, M. Balden, S. Lehwald, W. Daum, Surf. Sci. 360 (1996) 104–111.
[31] J. Zhao, H. Chen, X. Tian, H. Zang, Y. Fu, J. Shen, J. Catal. 298 (2013) 161–169.
[32] M.J. Lundwall, S.M. McClure, D.W. Goodman, J. Phys. Chem. C 114 (2010) 7904–7912.
[33] M.J. Kale, P. Christopher, ACS Catal. 6 (2016) 5599–5609.
[34] A. Walsh, J.L.F. Da Silva, S.-H. Wei, C. Körber, A. Klein, L.F.J. Piper, A. DeMasi, K.E. Smith, G. Panaccione, P. Torelli, D.J. Payne, A. Bourlange, R.G. Egdell, Phys. Rev. Lett. 100 (2008) 167402.
[35] H. Li, C. Chen, X. Huang, Y. Leng, M. Hou, X. Xiao, J. Bao, J. You, W. Zhang, Y. Wang, J. Song, Y. Wang, Q. Liu, G.A. Hope, J. Power Sources 247 (2014) 915–919.
[36] L. Zuo, Z. Gu, T. Ye, W. Fu, G. Wu, H. Li, H. Chen, J. Am. Chem. Soc. 137 (2015) 2674–2679.
[37] J. Mao, L. Ye, K. Li, X. Zhang, J. Liu, T. Peng, L. Zan, Appl. Catal. B: Environ. 144 (2014) 855–862.
[38] Z. Zhang, Z. Wang, S.-W. Cao, C. Xue, J. Phys. Chem. C 117 (2013) 25939–25947.
[39] N.M. Dimitrijevic, B.K. Vijayan, O.G. Poluektov, T. Rajh, K.A. Gray, H. He, P. Zapol, J. Am. Chem. Soc. 133 (2011) 3964–3971.
[40] X. Lin, Y. Yoon, N.G. Petrik, Z. Li, Z.-T. Wang, V.-A. Glezakou, B.D. Kay, I. Lyubinetsky, G.A. Kimmel, R. Rousseau, Z. Dohnálek, J. Phys. Chem. C 116 (2012) 26322–26334.
[41] Q. Wang, P. Dong, Z. Huang, X. Zhang, Chem. Phys. Lett. 639 (2015) 11–16.
[42] Q. Zhai, S. Xie, W. Fan, Q. Zhang, Y. Wang, W. Deng, Y. Wang, Angew. Chem. Int. Ed. 52 (2013) 5776–5779.
[43] Y.-C. Chen, Y.-C. Pu, Y.-J. Hsu, J. Phys. Chem. C 116 (2012) 2967–2975.
[44] R. Marschall, Adv. Funct. Mater. 24 (2014) 2421–2440.
[45] P.D.C. King, T.D. Veal, D.J. Payne, A. Bourlange, R.G. Egdell, C.F. McConville, Phys. Rev. Lett. 101 (2008) 116808.
[46] J. Zhao, Y. Wang, Y. Li, X. Yue, C. Wang, Catal. Sci. Technol. 6 (2016) 7967–7975.
[47] A. Corma, H. Garcia, J. Catal. 308 (2013) 168–175.
[48] P. Li, Y. Zhou, Z. Zhao, Q. Xu, X. Wang, M. Xiao, Z. Zou, J. Am. Chem. Soc. 137 (2015) 9547–9550.
[49] C.-C. Yang, J. Vernimmen, V. Meynen, P. Cool, G. Mul, J. Catal. 1 (2011) 1–8.
[50] S.-W. Cao, X.-F. Liu, Y.-P. Yuan, Z.-Y. Zhang, Y.-S. Liao, J. Fang, S.C.J. Loo, T.C. Sum, C. Xue, Appl. Catal. B: Environ. 147 (2014) 940–946.
[51] J. Cheng, M. Zhang, G. Wu, X. Wang, J. Zhou, K. Cen, Environ. Sci. Technol. 48 (2014) 7076–7084.
[52] J. Baltrusaitis, J. Schuttlefield, E. Zeitler, V.H. Grassian, Chem. Eng. J. 170 (2011) 471–481.
[53] H. Tsuneoka, K. Teramura, T. Shishido, T. Tanaka, J. Phys. Chem. C 114 (2010)

8892–8898.
[54] J. Ye, C. Liu, Q. Ge, J. Phys. Chem. C 116 (2012) 7817–7825.
[55] K. Bhattacharyya, A. Danon, K.B. Vijayan, K.A. Gray, P.C. Stair, E. Weitz, J. Phys. Chem. C 117 (2013) 12661–12678.
[56] D.A. Panayotov, P.A. DeSario, J.J. Pietron, T.H. Brintlinger, L.C. Szymczak, D.R. Rolison, J.R. Morris, J. Phys. Chem. C 117 (2013) 15035–15049.
[57] R. Long, Y. Li, Y. Liu, S. Chen, X. Zheng, C. Gao, C. He, N. Chen, Z. Qi, L. Song, J. Jiang, J. Zhu, Y. Xiong, J. Am. Chem. Soc. 132 (2017) 4486–4492.
[58] Y. Ji, Y. Luo, ACS Catal. 6 (2016) 2018–2025.
[59] Y. Ji, Y. Luo, J. Am. Chem. Soc. 138 (2016) 15896–15902.
[60] I.M.N. Groot, A.W. Kleyn, L.B.F. Juurlink, Angew. Chem. Int. Ed. 50 (2011) 5174–5177.
[61] M.J. Kolb, F. Calle-Vallejo, L.B.F. Juurlink, M.T.M. Koper, J. Chem. Phys. 140 (2014) 134708.
[62] J. Shen, J.M. Hill, R.M. Watwe, B.E. Spiewak, J.A. Dumesic, J. Phys. Chem. B 103 (1999) 3923–3934.
[63] J. Ye, C. Liu, D. Mei, Q. Ge, ACS Catal. 3 (2013) 1296–1306.
[64] C. Hahn, J. Shan, I.M.N. Groot, A.W. Kleyn, L.B.F. Juurlink, Catal. Today 154 (2010) 85–91.
[65] José L.C. Fajín, M.Natália DS Cordeiro, José R.B. Gomes, J. Phys. Chem. A 118 (2014) 5832–5840.
[66] H. He, P. Zapol, L.A. Curtiss, Energy Environ. Sci. 5 (2012) 6196–6205.